Microchimica Acta (2020) 187:207
https://doi.org/10.1007/s00604-020-4202-2

ORIGINAL PAPER

Electrochemical impedance biosensor array based on DNAzyme-functionalized single-walled carbon nanotubes using Gaussian process regression for Cu(II) and Hg(II) determination

Hui Wang[1,2] · Yang Liu[3] · Jun Wang[4] · Benhai Xiong[1] · Xiaopeng Hou[2]

Received: 11 October 2019 / Accepted: 28 February 2020
© Springer-Verlag GmbH Austria, part of Springer Nature 2020

Abstract

RNA-cleaving DNAzyme is a very useful biomaterial for metal ions determination. However, parts of DNAzymes can be cleaved by several metal ions, which makes it difficult to distinguish the concentrations of different metal ions. A method was applied to determine the Cu(II) concentration by using electrochemical biosensors combined with a mathematical model. An electrochemical biosensor was fabricated using single carbon nanotubes/field-effect transistor (SWNTs/FET) functionalized with a DNAzyme named PSCu10 and its complementary DNA embedded phosphorothioate RNA (CS-DNA). The CS-DNA with amino groups at the 5′ end was immobilized on the SWNTs' surface via the peptide bond and then combined with PSCu10 by identifying bases complementary pairing (Cuzyme/SWNTs/FET). The CS-DNA can be cleaved when Cu(II) bonded with the PSCu10 so that the structural change of Cuzyme improves the electrical conductivity of Cuzyme/SWNTs/FET. But CS-DNA also can be cut-off by the Hg(II) directly, which might interfere with the detection of the Cu(II) concentration using Cuzyme/SWNTs/FET. To solve this problem, Hgzyme/SWNTs/FET was employed to monitor the Hg(II) concentration at the same time, thus serving to determine the Cu(II) content through the Gaussian process regression. The biosensor array can determine the Cu(II) concentration varying from 0.01 to 10,000 nM when the Hg(II) concentration was ranging from 5 to 10,000 nM, and the limits of detection for Cu(II) and Hg(II) were 6.7 pM and 3.43 nM, respectively.

Keywords Impedance biosensor · Heavy metal · Field-effect transistor · Nanomaterial · Mathematical model

Introduction

Heavy metal contamination, especially mercury, cadmium, lead, copper, and chromium, has attracted numerous attention in developing countries. Heavy metal ions are easily absorbed by the plants via the natural environment and then enters the human or animal body through direct contact or food chains [1, 2]. Even though copper (Cu) at ultralow concentration plays critical structural and functional role in biological metabolism, it can cooperate with some proteins to form different proteases with specific function [3, 4]. Cu(II) exhibits as high toxic as Hg(II) when the levels of Cu(II) in the organs exceed an acceptable threshold [5], which will damage the normal function of the organs and cause adverse health effects [6, 7]. Therefore, it is crucial to determinate the concentrations of the Cu(II) and Hg(II) in the living environment and food.

So far, many standard methods to evaluate the concentration of Cu(II), such as atomic absorption/emission spectroscopy (AAS/AES) [8], inductively coupled plasma mass spectrometry (ICP-MS) [9], cold vapor atomic fluorescence

Electronic supplementary material The online version of this article (https://doi.org/10.1007/s00604-020-4202-2) contains supplementary material, which is available to authorized users.

✉ Hui Wang
wanghuilunwen@cau.edu.cn; wanghui_lunwen@163.com

✉ Xiaopeng Hou
houxiaopeng_lunwen@163.com

[1] State Key Laboratory of Animal Nutrition, Institute of Animal Sciences, Chinese Academy of Agricultural Sciences, Beijing 100193, People's Republic of China

[2] Research Institute of Wood Industry, Chinese Academy of Forestry, Beijing 100091, People's Republic of China

[3] School of Electronic and Information Engineering, Xi'an Jiaotong University, Xi'an 710049, People's Republic of China

[4] School of Agricultural Equipment Engineering, Henan University of Science and Technology, Luoyang, Henan Province 471003, People's Republic of China

Published online: 09 March 2020

spectrometry (CVAFS) [10], ultraviolet-visible spectroscopy (UV-vis) [11], and X-Ray fluorescence spectroscopy [12], rely on spectral technique. These approaches have high accuracy, stability, and sensitivity that are widely used in professional laboratories. Some new approaches based on fluorescence or colorimetric spectroscopy [13–15] were developed for the Cu(II) determination during these years. Electrochemical methods for the determination of heavy metal ions can overcome the shortages of the spectral approaches, due to small size devices, convenient operation, and low power consumption [16, 17].

Electrochemical sensor based on anodic stripping voltammetry is common method for the Cu(II) and Hg(II) determination [18]. Nonetheless, the stripping responses of Cu(II) and Hg(II) might overlap because the stripping potential of Cu(II) versus Ag/AgCl at − 0.15 V is close to the Hg(II) and Bi(III) [19], which will affect the accuracy.

In the past two decades, the rapid development of nanomaterials and biomaterials [20] offers more opportunity to improve the performances of electrochemical sensor. Many sensors for the Cu(II) and Hg(II) determination are fabricated using the small molecules, peptides, proteins, and antibodies, which have high sensitivity with low cost. (i) The ligand sites of proteases consisted by nitrogen, oxygen, or sulfur can combine with the heavy metal ions to form a stable complex, especially the sulfur atom of methionine (-SCH) and sulfhydryl group (-SH) of cysteine, but the protease-based biosensors lack the selective specificity that hard to distinguish Cu(II) with other heavy metal ions [21]. (ii) Cu(II) is a small ion that has to be chelated first and then bind to the antibody recognition, which may compromise selectivity [22]. Both antibody and enzyme work optimally under physiological conditions, which limit the application in the real environment.

DNA is not only the genetic material of most living organisms but also an excellent biological functional material [23]. Metal ions can specifically bind with a single-strand DNA to form a stable metal-mediated DNA, which this mechanism is applied to sense metal ions [24, 25]. Hence, numerous studies are primarily focused on the newly explored biosensor using different DNA-based aptamers functionalized with nanomaterials to improve the sensitivity. RNA-cleaving DNAzymes as DNA-based catalysts are obtained through in vitro selection that emerges as a very useful platform for the metal ions determination. Many biochemical and biophysical researches have been carried out on DNAzymes because of their high metal ion selectivity and high catalytic efficiency after bind with heavy metal ions [26]. Therefore, DNAzymes have been applied in electrochemical, colorimetric, and fluorescent biosensors that realize the detection of various metal ions such as Ag(I) [27], Mg(II) [28], Pb(II) [29], Hg(II) [16], Zn(II) [30], UO_2(II) [31], and paramagnetic metal ions such as Cu(II).

A DNAzyme-based biosensor was reported to sense the Cu(II) through indirect mean. The detection limit of this biosensor is 35 nM, but the detecting process is complicated because it requires ascorbate to reduce Cu(II) to Cu(I) [32]. Another Cu(II) sensor based on Cu(II)-dependent DNA-ligating DNAzyme is explored, which do not need any unstable substrates. Liu's group found a DNAzyme named PSCu10 [33], which had eight nucleotides in the enzyme loop with a cleavage rate of 0.1 min^{-1} in the presence of 1 μM Cu(II) at pH 6.0, can bind with Cu(II) to cleave the complementary DNA embedded phosphorothioate (PS) RNA. But the complementary DNA also can be cut off directly by the Hg(II) owing to its extremely high thiophilicity. Therefore, it is difficult to measure the Cu(II) concentration in real samples.

A biosensor array combined with Gaussian process regression to measure the Cu(II) and Hg(II) simultaneously, can conquer the insufficient specificity of PSCu10. The biosensor array was fabricated using single-gap field-effect transistor functionalized with SWNTs and DNAzyme via chemical bonding. The modification process was investigated through different spectral techniques including SEM, Raman, and UV-visible spectra, and the sensing performances were characterized by the linear voltammetry via exposing to a series of concentrations of Cu(II) and Hg(II) at room temperature. Due to Cuzyme/SWNTs/FET lacking specificity for Cu(II), it was difficult to distinguish the Cu(II) from the mixture solution. To solve this problem, Gaussian process regression was applied to process the data collected from the biosensor array to establish the mathematical model, which was further used to evaluate the Cu(II) concentration.

Materials and methods

Chemicals and materials

All of the nucleic acid chains were synthesized by the Shanghai Sangon Biological Engineering Technology & Services Co. Ltd. (Shanghai, China, https://www.sangon.com/). The sequences were:

Hgzyme: /AmC6/GrA*GCGCTArA*GAATrA*GCGCTC

PSCu10: GTTCGCCATCTTCACCAGGAAATAGT GACT

CS-DNA: /AmC6/AGTCACTATrA*GGAAGATG GCGAAC

CS-rDNA: /AmC6/AGTCACTATrAGGAAGAT GGCGAAC

CS-pDNA: /AmC6/AGTCACTATAGGAAGATGGC GAAC

The stock solutions of DNA/DNAzyme were prepared in Milli-Q water and quantified using UV-Vis absorption spectroscopy. The dispersed solution of single-wall carbon

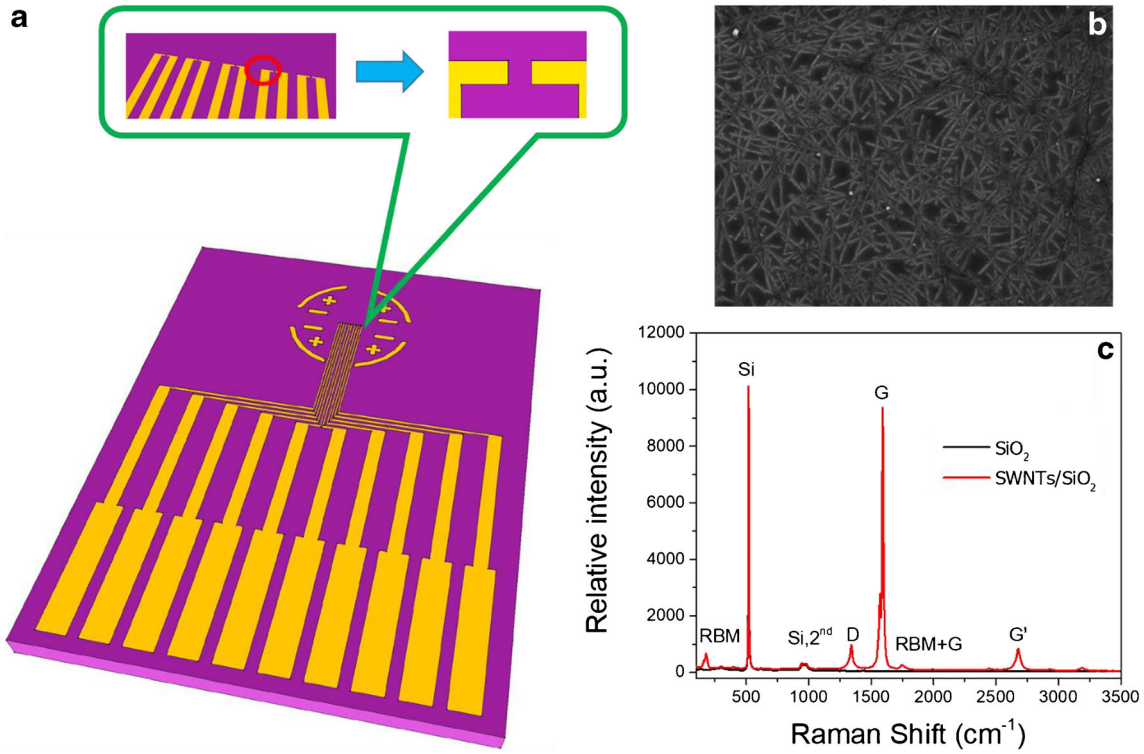

Fig. 1 **a**The microstructure of FET with five single-gap electrodes. **b** The SEM image of SWNTs/FET. **c** The Raman spectra of FET before and after functionalized SWNTs

nanotubes (SWNTs) was obtained from NanoIntegris Inc. (USA, http://nanointegris.com/), which the concentration was 0.01 mg/mL. Ethanolamine (EA, 99%) and 3-Aminopropyltriethoxysilane (APTES, 99%) were bought from Acros Organics (https://www.acros.com/). N, N-dimethylformamide (DMF, anhydrous, 99.8%), 6-mercapto-1-hexanol (MCH, 97%), and ethanolamine (EA) were purchased from Thermo Fisher, China (https://www.thermofisher.com/). Tween 20 was obtained from Bio-Rad. 2-(N-morpholino) ethanesulfonic acid (MES) and 3-(N-morpholino) propanesulfonic acid (MOPS) were offered by the Mandel Scientific Inc. (http://www.mandel.ca/). Standard solutions of K(I), Na(I), Pb(II), Cd(II), Zn(II), Cr(III), Fe(III), Cu(II), and Hg(II) were bought from Beijing Biaowu Technology Co., Ltd., China (http://www.biaowu.com/). The reaction buffer was pH 6.5, and the testing buffer was pH 7.4. Milli-Q water (electric resistance > 18.2 MΩ) obtained by sterilization process was used through this experiment (Billerica, MA, USA). Other reagents not mentioned were of analytical grade and used as received without further purification.

Apparatus

The properties of the biosensor array were performed by scanning electron microscope (SEM), Raman, UV-Vis spectrometer, current-voltage (I-V), and field-effect transistor (FET) measurement. For SWNTs/FET, the surface morphology and Raman spectra of SWNTs/FET were analyzed by scanning electron microscope (Zeiss Leo SUPRA 55, USA) and Dilor XY Laser Raman (532 nm Diode and Ar ion lasers), respectively. The UV spectrum was measured by Beckman DU4000 UV-visible spectrophotometer (Beckman Coulter, Inc. USA). I-V and FET measurements were collected by a semiconductor parameter analyzer (Keithley 2636, USA). For I-V measurement, the drain-source voltage was ramping from − 0.2 to + 0.2 V without gate bias ($V_G = 0$ V), and the current was recorded at the same time. The concentrations of DNA/DNAzyme solutions were evaluated based on the UV absorbance at 260 nm, which were calculated by the sum of the extinction coefficients of the individual bases.

Modification of the biosensor array

As shown in Fig. S1, the biosensor array was fabricated using a high doped p-type silicon wafer, which had a 100 nm thick thermal oxide (SiO_2) on the surface. Before photoresist coating preparation, the substrate was cleaned by acetone and isopropanol to remove the organic and inorganic impurities. The cleaned substrate has successively spun the photoresist, written the structure through standard lithographic patterning, and exposed under ultraviolet light. After baking, 20-nm-thick Cr and 180-nm-thick Au lays were E-beam evaporated. The deposited substrate was immersed in acetone overnight.

SWNTs/FET was prepared by the following steps. First, FET was rinsed with ammonium hydroxide and DI water, respectively. Next, the cleaned FET was immersed in 0.5 mL APTES for 30 min and rinsed with sufficient Milli-Q water. Then, the FET was covered with 0.01 mg/mL SWNTs solution, which was placed in high humidity for 60 min. Finally, SWNTs/FET was rinsed with Milli-Q water to remove the residues and was annealed at 250 °C using thermal chemical vapor deposition (CVD) in a lab-made horizontal tube furnace.

DNAzyme was functionalized with SWNTs/FET that comprised the steps listed below. SWNTs/FET was placed into 10 mM MCH in ethyl alcohol (0.5 mL) for 30 min that can block the gold surface, tread with a 6 mM PBASE dissolved in DMF (0.5 mL) for 60 min at room temperature, and rinsed with DMF and Milli-Q water to remove residues. Additionally, the treated SWNTs/FET was covered with 100 nM CS-DNA/Hgzyme solution (100 μL) for 8 h at 4 °C to immobilize CS-DNA/Hgzyme through the amide bond between the ester groups of PBASE and the amine at the 5′ end. To block the excess ester groups of PBASE and the exposed surface of SWNTs, 0.1 mM EA (100 μL) and 0.1% Tween 20 (100 μL) was employed to cover the surface of CS-DNA/SWNTs/FE or Hgzyme/SWNTs/FET. Finally, the CS-DNA/SWNTs/FET was hybridized with the 100 nM PSCu10 (100 μL) to form Cuzyme/SWNTs/FET.

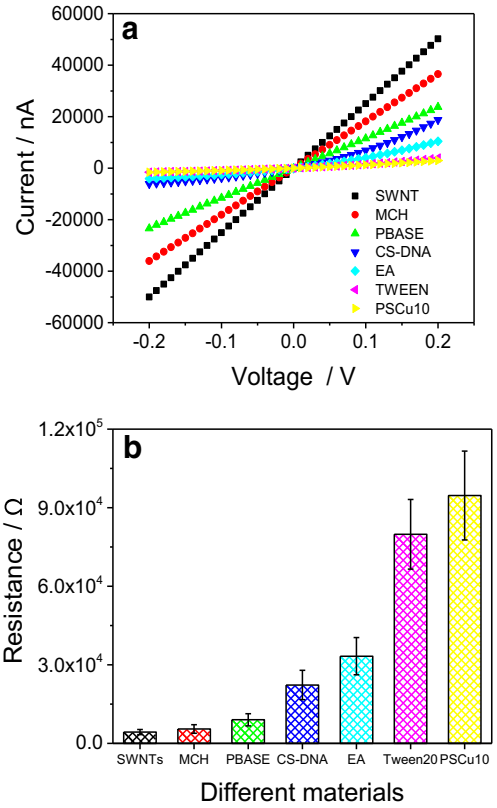

Fig. 2 **a** The I_{DS}–V_{DS} of FET modified with different materials (SWNTs, MCH, PBASE, CS-DNA, EA, Tween20, and PSCu10). **b** The resistances of FET modified with different materials at V_D = -0.02 V and V_G = 0 V. Each data point is an average of measurements from 5 independent biosensors

Sensing protocol

To evaluate the levels of Cu(II) and Hg(II), the biosensor array was immersed into the analyte liquor for 5 min and then cleaned with pH 7.4 buffer to remove the impurity ions. Furthermore, the biosensor array was covered with 50 μL pH 7.4 buffer and tested I-V using the Keithley 2636 source meter.

The relative resistance was defined as the following equation:

$$\triangle R/R\% = (R_0 - R)/R_0 \times 100\%$$

where R_0 was the initial resistance value and R was the resistance after explored to the analyte liquor.

Extract protocol

For the soil samples, the process was described as follows: (a) placing the soil samples in oven and heating at 100 °C to remove the moisture; (b) grinding the dried soil sample using a grinder; (c) weighing 2.0 g soil sample and then adding 0.1 M nitric acid; and (d) sonicating the mixture for 20 min and filtering the supernatant fluid with filter membrane. For the floor paint, the process was described as follows: (a) scraping the paint from the wooden floor; (b) grinding the paint sample and sieving using 0.5 mm sifter; (c) adding 0.2 g paint into 10 mL of an HCl solution; (d) the mixed solution was sonicated at room temperature for 60 min; and (e) the supernatant was filtered and then adjusted to pH 6.5.

Gaussian process regression

Gauss process regression (GPR) [34] based on a strict statistical learning theory is a machine learning regression method. GPR has been applied in many areas due to its adaptability to deal with complex problems such as high dimension, limited sample, and nonlinearity, which can obtain a distribution function.

With the dataset $D = \{X, Y\} = \{x_i, y_i\}_{i=1}^{n}$, the regression model can be formulated as:

$$y = f(x) + \varepsilon \quad (1)$$

where $f(\cdot)$ denotes an unknown regression function and ε is the Gaussian noise with zero mean and variance σ_n^2. The Gaussian process is completely specified by its mean function $m(x)$ and covariance function $C(x, x')$ from the function space view, which are defined as follows:

$$m(x) = E[f(x)] \quad (2)$$

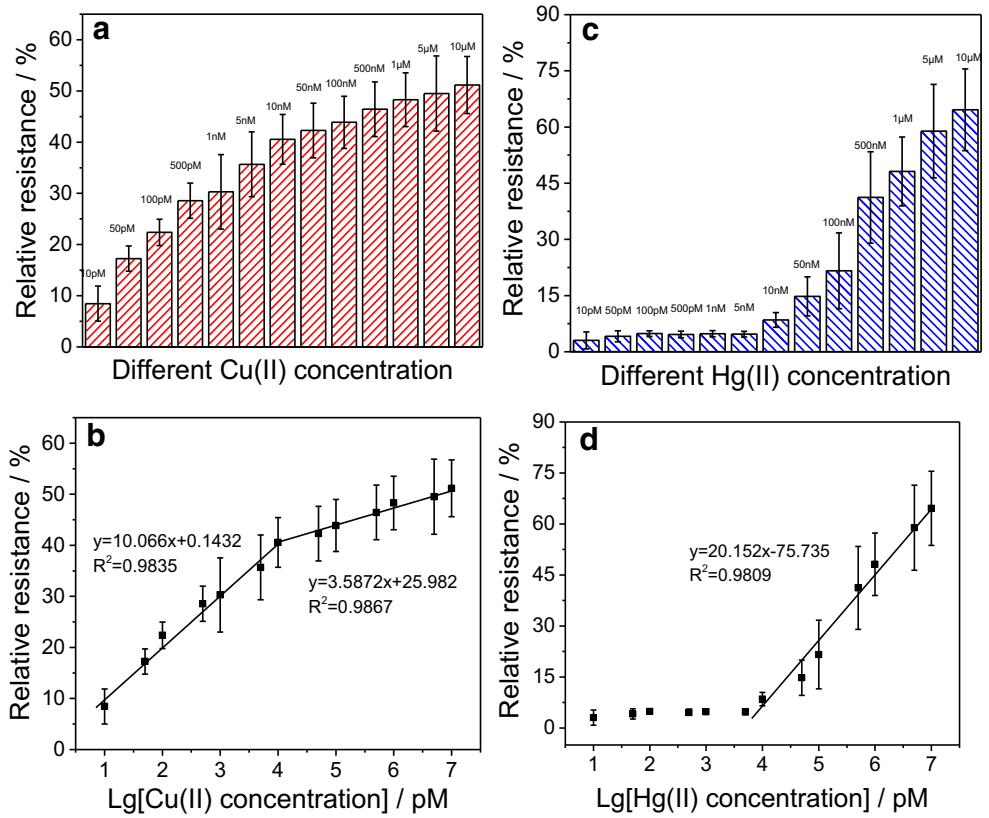

Fig. 3 **a** The relative resistance of Cuzyme/SWNTs/FET exposed to different Cu(II) concentrations (10, 50, 100, 500, 1000, 5000,10,000,50,000,100,000,500,000,1,000,000, 5,000,000, and 10,000,000 pM). **b** Linear regression of relative resistance vs. the logarithm of Cu(II) concentration. **c** The relative resistance of Hgzyme/SWNTs/FET exposed to different Hg(II) concentrations (10, 50, 100, 500, 1000, 5000,10,000,50,000,100,000,500,000,1,000,000, 5,000,000, and 10,000,000 pM). **d** Linear regression of relative resistance vs. the logarithm of Hg(II) concentration. The error bars indicate standard deviations from five biosensors

$$\left(x,x^{'}\right)=E\left[\left(f(x)-m(x)\right)\left(f\left(x^{'}\right)-m\left(x^{'}\right)\right)\right] \tag{3}$$

Then the Gaussian process can be denoted as:

$$f(x)\sim GP\left(m(x),C\left(x,x^{'}\right)\right) \tag{4}$$

Usually, the data is normalized for notation simplicity, and then the output observations follow a Gaussian distribution as:

$$y\sim GP\left(0,C\left(x,x^{'}\right)\right) \tag{5}$$

When a query input x_* comes in, the joint distribution of the training outputs y and the test output y_* according to the prior is

$$\begin{bmatrix} y \\ y_x \end{bmatrix}\sim N\left(0,\begin{bmatrix} c & k^{*} \\ k^{T} & C(x_*,x_*) \end{bmatrix}\right) \tag{6}$$

where $k_*=[C(x_*,x_1),\cdots,C(x_*,x_n)]^T$. Then the prediction output (y_*) and variance ($\sigma_*{}^2$) can be given as:

$$\begin{cases} y^{*}=k_*^T \\ \sigma_*{}^2=C(x_*,x_*)-k_*^T C^{-1}k_* \end{cases} \tag{7}$$

Results

Choice of materials

FET makes the biosensor array more easily to achieve miniaturization, fast response time, and mass production with low cost. Due to unique physicochemical properties, many materials, including SWNT, graphene, rGO, and MoS_2, have been modified on the FET's surface to develop different sensing devices. In comparison, SWNT/FET was easily prepared with excellent mechanical stability and chemical stability.

Characterization

Figure 1 a shows that the single-gap structure was written on the chip surface, which contained five single-gap electrodes. Both the width and length of the single-gap electrode were 10 μm. After SWNTs were functionalized on the area between drain and source using the protocol in 2.3, the characteristics were investigated by SEM and Raman. The SEM image of SWNTs/FET is shown in Fig. 1b. It was clear that the surface was covered with a complex network

structure, indicating SWNTs were uniformly immobilized on the FET's surface. Figure 1c displays the Raman spectrum of bare FET and SWNTs/FET. Only two bands were found on the Raman spectra of bare FET (black curve) ranging from 200 to 3500 cm^{-1}, which located at 600 cm^{-1} and 956 cm^{-1}, respectively. According to the literature, they were Si band and Si 2nd band. When SWNTs were connected to the FET' surface by the silane-coupling agent of APTES, there were several bands with high intensity on the Raman spectra of SWNTs/FET. These bands were located at 178 cm^{-1}, 1345 cm^{-1}, 1592 cm^{-1}, and 2682 cm^{-1}, which were identified with RBM-band, D-band, G-band, and G'-band of SWNTs that correspond to carbon stretching modes of sp2 and sp3, respectively.

Figure 2 shows the currents and voltages after SWNTs functionalized with MCH, PBASE, CS-DNA, EA, Tween20, and PSCu10. During the process of immobilization, I_{DS} displayed a downward trend which was a nonlinear and positive correlation with V_{DS}. It indicated that these chemical molecules or biomolecules had been combined with gold or SWNTs. The resistances at each voltage were calculated using Ohm's law, which were linear with voltages in Fig. S3. After SWNTs/FET incubated in MCH solution, the resistance value increased slightly in the view of MCH only bound with Au to form a nonconductive membrane. For other molecules, they were functionalized on the SWNTs' surface through different bonds and affected the electrical conductivity of SWNTs. The pyrene of PBASE was attached with SWNTs due to the C–C bond through π–π interaction. CS-DNA with the amine was covalent with the ester group of PBASE. EA and Tween20 were used to block the unbind PBASE and bare SWNTs' surface to prevent the absorbing impurities. The number of charge carrier in SWNTs was easily affected by PBASE, CS-DNA, EA, Tween20, and PSCu10, attributing to electron donation or electron scattering.

Sensitivity for the Cu(II) and Hg(II) determination

To obtain the linearity region, the biosensor array was exposed to different concentrations of Cu(II) and Hg(II) in 50 mM MOPS buffer, respectively. Under the optimal conditions discussed above, the detecting data is shown in Fig. 3. The relative resistances of Cuzyme/SWNTs/FET were growing up along with the increasing concentrations of Cu(II), which exhibited a positive relationship, indicating that Cuzyme on the SWNTs' surface was cleaved by the Cu(II). There are two segments that the relative resistances were linear with the logarithm of Cu(II) concentration in the range of 10 to 10,000 pM and 10,000 to 10,000,000 pM. The regression equations were $y_1 = 10.066x + 0.1432$ and $y_2 = 3.5872x + 25.982$ with the limit of detection 6.7 pM (N/S = 3), which the linear regression correlation coefficients

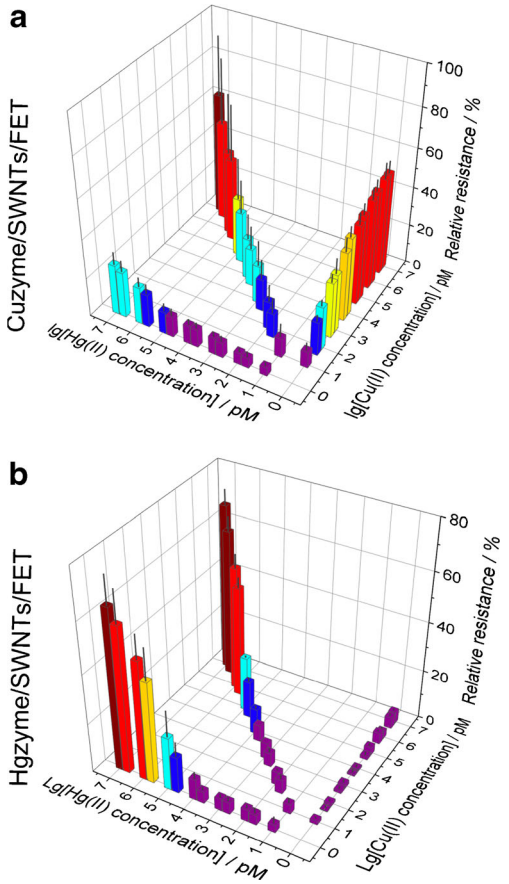

Fig. 4 The relative resistance of (**a**) Cuzyme/SWNTs/FET and (**b**) Hgzyme/SWNTs/FET exposed to different mixtures of Cu(II) and Hg(II) (0–10, 0–50, 0–100, 0–500, 0–1000, 0–5000, 0–10,000, 0–50,000, 0–100,000, 0–500,000, 0–1,000,000, 0–5,000,000, and 0–10,000,000 pM; 10–0, 50–0, 100–0, 500–0, 1000–0, 5000–0, 10,000–0, 50,000–0, 100,000–0, 500,000–0, 1,000,000–0, 5,000,000–0, and 10,000,000–0 pM; and 10–10, 50–50, 100–100, 500–500, 1000–1000, 5000–5000,10,000–10,000, 50,000–50,000, 100,000–100,000, 500,000–500,000, 1,000,000–1,000,000, 5,000,000–5,000,000, and 10,000,000–10,000,000 pM). The error bars indicate standard deviations from five biosensors

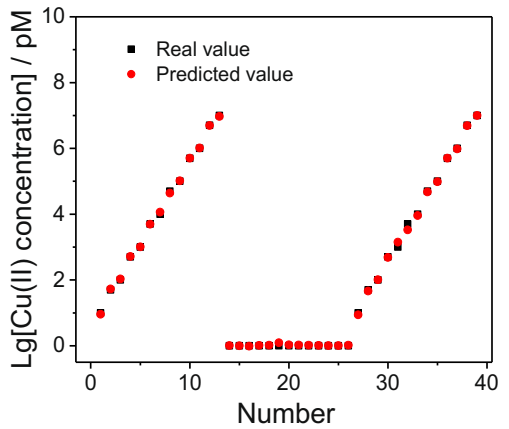

Fig. 5 The real value versus the predicted value calculated by the GPR

Table 1 Compare the detecting performances of the biosensor array with other sensors

Sensor	Method	Metal Ion	Linear range (nM)	Low of detection (nM)	Time (min)	Reference
TFME	DPASV	Cd(II)	5.4–89.3	0.54	5	[35]
		Cu(II)	2.5–156	0.31		
		Pb(II)	2.9–48.3	0.14		
		Zn(II)	15.4–153.8	9.23		
C-dots	UV-vis	Cu(II)	10–5000	5	10–15	[36]
NG/GCE	DPSV	Cd(II)	50–9000	30	5	[37]
		Pb(II)	7–9000	2		
		Cu(II)	9–5000	1		
		Hg(II)	70–9000	10		
PAAM/PA/PDA	DPV	Cu(II)	1–1000	25	0.17	[38]
CPME	DPAdSV	Cu(II)	1500–31,000	400	30	[39]
Mo6S9-xIx/GCE	DPASV	Cu(II)	7.8–2343.8	2.5	4	[40]
		Pb(II)	7.2–2173.9	2.17		
		Cd(II)	7.1–2142.8	1.78		
Biosensor array	IV	Cu(II)	0.01–10,000	0.0064	5	This work
		Hg(II)	10–10,000	3.43		

were 0.992 and 0.993, respectively. Besides, the relative resistances of Hgzyme/SWNTs/FET were not changed when the Hg(II) concentration was lower than 5000 pM. The regression equation was $y = 20.152x - 75.735$ in the range of 5000 pM to 10,000,000 pM, and the detection limit was 3.43 nM.

Data analysis methods

Data preparation

Cuzyme/SWNTs/FET was sensitive to the Cu(II) and Hg(II), which made it hard to determine the level of Cu(II) accurately. Therefore, Hgzyme/SWNTs/FET was employed to monitor the Hg(II) concentration. This biosensor array was employed to measure the different mixtures of Cu(II) and Hg(II), and the detecting results are shown in Fig. 4.

Data preprocessing

Data were preprocessed to select accurate and reliable ones as modeling data. The data mainly included errors or negative data deletions. To eliminate the influence of the different orders of magnitude and improve network convergence performance, sample data should generally be normalized. The output variables were normalized based on Eq. (1), as follows:

$$Y = [12 + log_{10}(C)]/12 \quad (8)$$

$$X = \left[1, x_1, {x_1}^2, x_2, , {x_2}^2, x_1 * x_2\right] \quad (9)$$

where C is the concentration of Cu(II) and Hg(II), Y_{max} represents the maximum value of the variable, and Y_{min} presents its minimum value. x_1 was the relative resistance of Cuzyme/SWNTs/FET, and x_2 was the relative resistance of Cuzyme/SWNTs/FET.

Table 2 Determination of Cu(II) and Hg(II) in real samples using the biosensor array and ICP-MS.

Sample	Add Hg(II)	The biosensor array		ICP-MS		Recovery (%)	
		Cu(II)	Hg(II)	Cu(II)	Hg(II)	Cu(II)	Hg(II)
Pait 1	10 nM	14.32 ± 3.62 nM	10.53 ± 2.34 nM	15.35 nM	10.11 nM	94.02	104.2
Pait 2	10 nM	12.13 ± 3.45 nM	10.23 ± 3.31 nM	12.96 nM	10.34 nM	93.60	98.93
Pait 3	10 nM	24.50 ± 5.48 nM	11.23 ± 2.21 nM	26.25 nM	10.56 nM	93.33	106.3
Soil 1	10 nM	2.32 ± 0.46 μM	102.1 ± 10.22 nM	2.16 μM	108.6 nM	107.5	93.05
Soil 2	10 nM	3.45 ± 0.83 μM	140.5 ± 23.3 nM	3.58 μM	144.3 nM	96.37	97.02
Soil 3	10 nM	2.57 ± 0.62 μM	232.1 ± 29.2 nM	2.69 μM	251.4 nM	95.54	92.32

Gaussian process regression

Gaussian process regression was used to build the prediction model. The X matrix consisting of 39 rows and 6 columns was used as the workspace variable, and the Y matrix consisted of 39 rows and 1 column was selected as the response. After the model was established, the predicted values from the GPR are compared to the true values, which were exhibited in Fig. 5. The correlation coefficient (R_0) and root mean square error (RSMT) between real concentrations and predicted concentrations were 0.985 and 0.038, indicating the forecast precision of GPR trained was more precise in prediction and then predicting result was reliable.

Table 1 shows the performance parameters of the biosensor array, containing the linear range, the limit of detection, and detection time. Even though the detection time was longer than some of the sensors, the linear range and limit detection for the Cu(II) and Hg(II) were superior to the mentioned sensors.

Real sample analysis

To evaluate the applicability, the biosensor array was used to measure the real samples collected from the indoor and outdoor environments. The proposed biosensor array can only be used to determine heavy metal ions in liquid so that Cu(II) and Hg(II) need to be extracted from the samples using the protocol in 2.5. All the samples were measured using biosensor arrays and inductively coupled plasma mass spectrometry (ICP-MS), and the results were listed in Table 2. Compared to the recoveries of Cu(II) and Hg(II), it was found that the relative errors were lower than 10%. It demonstrated that results from biosensor array were in good agreement with those obtained using ICP-MS.

Conclusion

A new biosensor array based on SWNTs/FET functionalized with RNA-cleaving DNAzyme was developed, which was applied to determine the contents of Cu(II) and Hg(II). The biosensor modification process was characterized by using SEM, Raman spectra, UV-visible spectrum, and current-voltage, indicating that different materials were modified on the FET's surface successfully. The sensing properties and cross-sensitive characteristics of the biosensor array towards Cu(II) and Hg(II) were investigated at room temperature, and the detecting data was processed using Gaussian process regression to establish a mathematical processing model. To measure the real samples, the biosensor array for the Cu(II) and Hg(II) determination had excellent sensitivity, selectivity, practicability, and stability. This work offered a new way to improve the practicability of DNAzyme with poor selectivity.

Funding information This work was supported by the Key Realm R&D Program of Guangdong Province (No. 2019B020215004 and No. 2019B020215002), the Science and Technology Major Project of Guangxi Province (GUIKE AA17204087-13), and the Chinese National Natural Science Foundation (No. 31671578).

Compliance with ethical standards

Conflict of interest The authors declare that they have no conflict of interest.

References

1. Nazir R, Khan M, Masab M, Rehman HU, Rauf NU, Shahab S, Ameer N, Sajed M, Ullah M, Rafeeq M (2015) Accumulation of heavy metals (Ni, Cu, Cd, Cr, Pb, Zn, Fe) in the soil, water and plants and analysis of physico-chemical parameters of soil and water collected from Tanda Dam Kohat. J Pharm Sci Res 7:89–97
2. Copaja SV, Pérez CA, Vega-Retter C, Véliz D (2017) Heavy metal content in Chilean fish related to habitat use, tissue type and river of origin. B Environ Contam Tox 99(6):695–700
3. Beedle AE, Lezamiz A, Stirnemann G, Garcia-Manyes S (2015) The mechanochemistry of copper reports on the directionality of unfolding in model cupredoxin proteins. Nat Commun 6(1):1–9
4. Knop M, Dang TQ, Jeschke G, Seebeck FP (2017) Copper is a cofactor of the formylglycine-generating enzyme. ChemBioChem 18(2):161–165
5. Ahmed Q, Bat L, Yousuf F (2017) Contamination of Cu, Zn, Fe and Mn in Katsuwonus pelamis (Linnaeus, 1758) from Karachi fish harbor and potential risks to human health. Int J Marine Sci 7:76–87
6. Ahuja A, Dev K, Tanwar RS, Selwal KK, Tyagi PK (2015) Copper mediated neurological disorder: visions into amyotrophic lateral sclerosis, Alzheimer and Menkes disease. J Trace Elem Med Biol 29:11–23
7. Dusek P, Roos PM, Litwin T, Schneider SA, Flaten TP, Aaseth J (2015) The neurotoxicity of iron, copper and manganese in Parkinson's and Wilson's diseases. J Trace Elem Med Biol 31: 193–203
8. Özzeybek G, Erarpat S, Chormey DS, Fırat M, Büyükpınar Ç, Turak F, Bakırdere S (2017) Sensitive determination of copper in water samples using dispersive liquid-liquid microextraction-slotted quartz tube-flame atomic absorption spectrometry. Microchem J 132:406–410
9. Drobyshev EJ, Solovyev ND, Ivanenko NB, Kombarova MY, Ganeev AA (2017) Trace element biomonitoring in hair of school children from a polluted area by sector field inductively coupled plasma mass spectrometry. J Trace Elem Med Biol 39:14–20
10. Hu J, Sturgeon RE, Nadeau K, Hou X, Zheng C, Yang L (2018) Copper ion assisted photochemical vapor generation of chlorine for its sensitive determination by sector field inductively coupled plasma mass spectrometry. Anal Chem 90(6):4112–4118
11. Stiedl J, Green S, Chassé T, Rebner K (2019) Characterization of oxide layers on technical copper material using ultraviolet visible (UV–Vis) spectroscopy as a rapid on-line analysis tool. Appl Spectrosc 73(1):59–66
12. Meira LA, Almeida JS, Dias FDS, Pedra PP, Pereira ALC, Teixeira LS (2018) Multi-element determination of Cd, Pb, Cu, V, Cr, and Mn in ethanol fuel samples using energy dispersive X-ray fluorescence spectrometry after magnetic solid phase microextraction using $CoFe_2O_4$ nanoparticles. Microchem J 142:144–151
13. He Y, Tian F, Zhou J, Jiao B (2019) A fluorescent aptasensor for ochratoxin a detection based on enzymatically generated copper

nanoparticles with a polythymine scaffold. Microchim Acta 186(3): 199
14. Shahdordizadeh M, Yazdian-Robati R, Ansari N, Ramezani M, Abnous K, Taghdisi SM (2018) An aptamer-based colorimetric lead (II) assay based on the use of gold nanoparticles modified with dsDNA and exonuclease I. Microchim Acta 185(2):151
15. Tang Z, Zhang H, Ma C, Gu P, Zhang G, Wu K, Wang K (2018) Colorimetric determination of the activity of alkaline phosphatase based on the use of Cu (II)-modulated G-quadruplex-based DNAzymes. Microchim Acta 185(2):109
16. Wang H, Liu Y, Liu G (2018) Electrochemical biosensor using DNA embedded phosphorothioate modified RNA for mercury ion determination. ACS Sens 3(3):624–631
17. Wang H, Zhao G, Zhang Z, Yi Y, Wang Z, Liu G (2017) A portable electrochemical workstation using disposable screen-printed carbon electrode decorated with multiwall carbon nanotube-ionic liquid and bismuth film for Cd (II) and Pb (II) determination. Int J Electrochem Sci 12:4702–4713
18. Guo Z, Luo XK, Li YH, Zhao QN, Li MM, Zhao YT, Ma C (2017) Simultaneous determination of trace Cd (II), Pb (II) and Cu (II) by differential pulse anodic stripping voltammetry using a reduced graphene oxide-chitosan/poly-l-lysine nanocomposite modified glassy carbon electrode. J Colloid Interface Sci 490:11–22
19. Mohadesi A, Taher MA (2007) Voltammetric determination of Cu (II) in natural waters and human hair at a meso-2, 3-dimercaptosuccinic acid self-assembled gold electrode. Talanta 72(1):95–100
20. Oh WK, Kwon OS, Jang J (2013) Conducting polymer nanomaterials for biomedical applications: cellular interfacing and biosensing. Polym Rev 53(3):407–442
21. Syshchyk O, Skryshevsky VA, Soldatkin OO, Soldatkin AP (2015) Enzyme biosensor systems based on porous silicon photoluminescence for detection of glucose, urea and heavy metals. Biosens Bioelectron 66:89–94
22. Ouyang H, Shu Q, Wang W, Wang Z, Yang S, Wang L, Fu Z (2016) An ultra-facile and label-free immunoassay strategy for detection of copper (II) utilizing chemiluminescence self-enhancement of Cu (II)-ethylenediaminetetraacetate chelate. Biosens Bioelectron 85: 157–163
23. Seeman NC, Sleiman HF (2017) DNA nanotechnology. Nat Rev Mater 3(1):1–23
24. Wang H, Liu Y, Liu G (2018) Reusable resistive aptasensor for Pb(II) based on the Pb(II)-induced despiralization of a dna duplex and formation of a G-quadruplex. Microchim Acta 185(2):142
25. Liu L, Wu HC (2016) Dna-based nanopore sensing. Angew Chem Int Ed 55(49):15216–15222
26. Liang G, Man Y, Li A, Jin X, Liu X, Pan L (2017) Dnazyme-based biosensor for detection of lead ion: a review. Microchem J 131:145–153
27. Wang H, Liu Y, Liu G (2018) Label-free biosensor using a silver specific RNA-cleaving DNAzyme functionalized single-walled carbon nanotube for silver ion determination. Nanomaterials 8:258
28. Liu S, Cheng C, Gong H, Wang L (2015) Programmable Mg^{2+}-dependent DNAzyme switch by the catalytic hairpin DNA assembly for dual-signal amplification toward homogeneous analysis of protein and DNA. Chem Commun 51(34):7364–7367
29. Wang H, Yin Y, Gang L (2019) Single-gap microelectrode functionalized with single-walled carbon nanotubes and Pbzyme for the determination of Pb^{2+}. Electroanal 31(6):1174–1181
30. Shen W, Li Y, Qi T, Wang S, Sun J, Deng H, Tang S (2018) Fluorometric determination of zinc (II) by using DNAzyme-modified magnetic microbeads. Microchim Acta 185(10):447
31. Gupta VK, Singh AK, Kumawat LK, Mergu N (2016) An easily accessible switch-on optical chemosensor for the detection of noxious metal ions Ni(ii), Zn(ii), Fe(iii) and Uo_2(ii). Sensor Actuat B-Chem 222:468–482
32. Liu M, Zhao H, Chen S, Yu H, Zhang Y, Quan X (2011) A "turn-on" fluorescent copper biosensor based on dna cleavage-dependent graphene-quenched dnazyme. Biosens Bioelectron 26(10):4111–4116
33. Huang PJJ, Liu J (2016) An ultrasensitive light-up Cu^{2+} biosensor using a new DNAzyme cleaving a phosphorothioate-modified substrate. Anal Chem 88(6):3341–3347
34. Yang K, Jin H, Chen X, Dai J, Wang L, Zhang D (2016) Soft sensor development for online quality prediction of industrial batch rubber mixing process using ensemble just-in-time Gaussian process regression models. Chemometr Intell Lab 155:170–182
35. Kudr J, Nguyen H, Gumulec J, Nejdl L, Blazkova I, Ruttkay-Nedecky B, Hynek D, Kynicky J, Adam V, Kizek R (2015) Simultaneous automatic electrochemical detection of zinc, cadmium, copper and lead ions in environmental samples using a thin-film mercury electrode and an artificial neural network. Sensors 15: 592–610
36. Gangaraju G, Wu HF, Lee CY (2015) Green synthesis of carbon dots from prawn shells for highly selective and sensitive detection of copper ions. Sensor Actuat B-Chem 224:396–403
37. Xing H, Xu J, Zhu X, Duan X, Lu L, Wang W, Zhang Y, Yang T (2016) Highly sensitive simultaneous determination of cadmium (II), lead (II), copper (II), and mercury (II) ions on N-doped graphene modified electrode. J Electroanal Chem 760:52–58
38. Zhao Z, Chen H, Zhang H, Ma L, Wang Z (2017) Polyacrylamide-phytic acid-polydopamine conducting porous hydrogel for rapid detection and removal of copper (II) ions. Biosens Bioelectron 91: 306–312
39. Oliveira PR, Lamy-Mendes AC, Mangrich AS, Junior LHM, Bergamini MF (2015) Electrochemical determination of copper ions in spirit drinks using carbon paste electrode modified with biochar. Food Chem 171:426–431
40. Hong L, Li M, Mihailovič D (2015) Simultaneous determination of copper, lead, and cadmium ions at a Mo 6 S 9-x I x nanowires modified glassy carbon electrode using differential pulse anodic stripping voltammetry. Electrochim Acta 154:184–189

Publisher's note Springer Nature remains neutral with regard to jurisdictional claims in published maps and institutional affiliations.